THE JOURNAL OF PHYSICAL CHEMISTRY B

ARTICLE

pubs.acs.org/JPCB

Nonergodicity Factor, Fragility, and Elastic Properties of Polymeric Glassy Sulfur

B. Ruta,[†] G. Monaco,[*,†] V. M. Giordano,[†,‡] F. Scarponi,[§,∥] D. Fioretto,[§,∥] G. Ruocco,[§,⊥] K. S. Andrikopoulos,[#,▽] and S. N. Yannopoulos[▽]

[†]European Synchrotron Radiation Facility, BP220, F-38043, Grenoble, France

[‡]LPMCN, Université Claude Bernard Lyon 1 and CNRS, 69622, Villeurbanne, France

[§]CNR-IPCF, Rome University "La Sapienza", Piazzale A. Moro 2, I-00185 Roma, Italy

[∥]Department of Physics, Perugia University, Via A. Pascoli, I-06100 Perugia, Italy

[⊥]Department of Physics, Rome University "La Sapienza", Piazzale A. Moro 2, I-00185 Roma, Italy

[#]Department of Applied Sciences, Technological Educational Institute of Thessaloniki, 57400 Sindos, Greece

[▽]Foundation for Research and Technology Hellas, Institute of Chemical Engineering and High Temperature Chemical Processes (FORTH/ICE-HT), P.O. Box 1414, GR-26504 Patras, Greece

ABSTRACT: We present a detailed investigation of the vibrational dynamics of glassy sulfur (g-S). The large frequency range spanned in this study has allowed us to carefully scrutinize the elastic properties of g-S and to analyze their relation to various features of both the glassy and the liquid state. In particular, the acoustic properties of g-S present a quasi-harmonic behavior in the THz frequency range, while at lower frequency, in the GHz range, they are affected by a strong anharmonic contribution. Moreover, the high frequency (THz) dynamics of g-S does not present signatures of the elastic anomalies recently observed in a number of glasses. Despite this apparent contradiction, we show that this finding is not in disagreement with the previous ones. Finally, by considering the correct long wavelength limit of the density fluctuations in the glassy state, we estimate the continuum limit of the nonergodicity factor and we investigate recently proposed relations between the fast dynamics of glasses and the slow dynamics of the corresponding viscous melts.

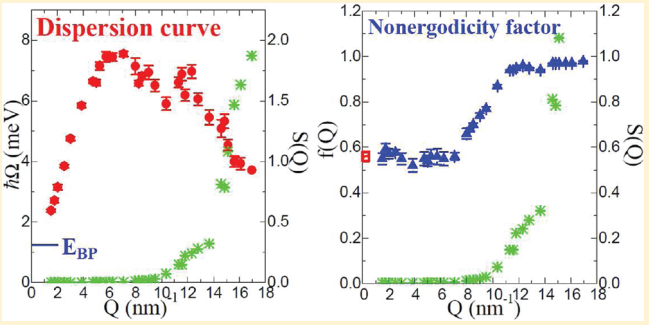

1. INTRODUCTION

Glass forming systems are characterized by a rich phenomenology both in the supercooled and in the glassy state.[1] In the last decades, numerous researchers have tried to find an answer to challenging open questions like the most general "what is the nature of the glass transition" or "if the dynamics in the glassy state is simply connected to that in the liquid phase", or to questions more specific to the glassy state such as "what is the origin of the universal thermal anomalies at low temperature in glasses" and "what is the role played by the corresponding acoustic excitations". However, despite the large efforts done in the field, many aspects remain poorly clarified and the understanding of the glassy state is still considered as one of the most challenging topics in condensed matter physics.[1]

Many of the above-mentioned questions require a detailed knowledge of the vibrational properties of glasses on different length scales. This information can be obtained by studying the dynamic structure factor, $S(Q,\hbar\omega)$, of a glass in the macroscopic limit, e.g., in the ∼GHz frequency range, by means of Brillouin light scattering (BLS), and in the microscopic one, thus in the THz frequency range, by means of inelastic X-ray scattering (IXS).

For instance, the information on the elastic properties of a glass can be used to study the proposed connection between the vibrational dynamics of glasses and the relaxational dynamics in the corresponding supercooled liquids close to the glass transition.[2−8] There, the relaxational dynamics shows a huge slowdown that can be quantitatively grasped by the fragility parameter, m_A, which in its kinetic version describes how fast the viscosity, or the structural relaxation time, increases with decreasing temperature on approaching the glass transition temperature T_g.[9,10] The proposed connection between m_A and the elastic properties of a glass is fascinating, as it implies that the fast vibrational dynamics in a glass is fixed by the slow relaxational dynamics in the corresponding melt.

The comprehension of the vibrational dynamics of a glass, in particular at high frequencies, contains moreover the promise to shed some light on one of the most intriguing features of the

Special Issue: H. Eugene Stanley Festschrift

Received: April 20, 2011
Revised: September 23, 2011
Published: October 18, 2011

glassy state itself. Indeed, it is well known that the vibrational density of states (VDOS) $g(\omega)$ of a glass is characterized by the presence of an excess of modes over the $\sim\omega^2$ Debye continuum model prediction which is related to the universal thermal anomalies present at low temperature in glasses.[11] This excess of vibrational states, called the "boson peak" (BP), is universal in glasses and appears as a characteristic broad asymmetric peak, at frequencies of ~1 THz, when plotting the reduced density of states $g(\omega)/\omega^2$ as a function of the excitation energy.[12] Albeit the BP has been studied for more than 40 years, no agreement exists yet on its physical origin and it still remains the subject of an increasing number of theoretical[13−18] and experimental[19−27] works. There is a general agreement that the boson peak is related to the structural disorder, but the main question of whether this peak depends or not on a peculiar behavior of the high frequency acoustic excitations present in the corresponding energy range is still unanswered.

In this paper, we present a detailed investigation of the vibrational properties of elemental glassy sulfur (g-S). The vibrational dynamics has been studied in the high frequency range by means of IXS and is here reported together with a detailed analysis of the corresponding macroscopic behavior previously probed with BLS.[28] The combined use of low and high frequency data has allowed us to carefully scrutinize the elastic properties of the system and to analyze their relation to the above-mentioned features in the liquid and the glassy state, i.e., the fragility and the boson peak, respectively. Moreover, we show that by combing the elastic properties on different length scales it is possible to have a clear view of the vibrational dynamics of the system. For instance, the knowledge of the macroscopic behavior is fundamental for the understanding of the acoustic excitations in the crucial frequency range explored by IXS. In the case of sulfur, we find that at high frequencies the acoustic dynamics does not display any signature of the elastic anomalies recently found in other glasses which appear to be strictly related to the boson peak.[29−32] Notwithstanding this finding is not in disagreement with the previous ones, and can instead explain also the absence of such anomalies in few other glasses.

This paper is structured as follows. In sections 2 and 3, we present the details of the experiment, sample preparation procedure, and data treatment. The high frequency acoustic excitations are then discussed in relation to both the excess of modes in the VDOS (section 4.1) and the corresponding low frequency data (section 4.2). The knowledge of the vibrational dynamics of the glass in a wide frequency range and the detailed analysis of the IXS spectra are then used, in section 4.3, to get information on the macroscopic limit of the nonergodicity factor in the glass through the estimation of the isothermal compressibility in the corresponding viscous liquid at T_g. Following a study reported in ref 28, the information on the elastic properties and on the isothermal compressibility has been used to compare the dynamics of the glass to that of the corresponding polymeric liquid at high temperature (section 4.4). Finally, the behavior of the nonergodicity factor has been used in section 4.5 to carefully investigate its relation to the kinetic fragility of the corresponding supercooled liquid, estimated by considering the presence of an important secondary relaxation process in the liquid phase close to T_g.

2. EXPERIMENTAL DETAILS

2.1. The Technique. Inelastic X-ray scattering measurements were carried out at the very high energy resolution beamline ID16 at the European Synchrotron Radiation Facility in Grenoble. An incident beam with an energy of 23.724 keV has been used, monochromatized using a flat perfect single Si crystal operated at a Bragg angle of 89.98° and at the (12,12,12) reflection order. The photons scattered by the sample have been collected by an array of five analyzers which focus them on independent detectors. The analyzers work in the same configuration as the main monochromator, and allow for the collection of five spectra corresponding to different momentum transfers simultaneously. The overall energy resolution of the spectrometer was 1.3−1.5 meV full width at half-maximum (fwhm), depending on the analyzer crystal, and was determined from elastic scattering measurements from a plexiglass sample at low temperature. The energy scans were performed varying the temperature of the monochromator and keeping the temperature of the analyzers fixed. The Q-resolution was defined by slits in front of the analyzers and was kept to ~0.34 nm^{-1}. Each scan was performed in the −30/+30 meV energy range around the elastic line by using a step of 0.2 meV in the central part of the spectrum (−20/+20 meV) and a step of 0.4 meV in the tails. The measurements were performed at T = 101, 148, and 202 K. Concerning the first two temperatures, the dynamic structure factor, $S(Q,\hbar\omega)$, has been measured only at five different Q-values, corresponding to the five analyzers at one setting of the spectrometer arm, with a fixed distance in Q of ~3.3 nm^{-1} one from the other. At T = 202 K, the IXS spectra have been collected in the exchanged momentum, Q, range between 1.5 and 17 nm^{-1}, thus up to values close to the first maximum in the static structure factor (~18 nm^{-1}). Depending on the investigated temperature, each point of the spectra was counted between 180 and 360 s in order to reach an acceptable signal-to-noise ratio.

2.2. Sample Preparation. Elemental sulfur is one of the most thoroughly studied elements owing to its impressive properties in both the crystalline and the liquid phase.[33] Crystalline sulfur melts in a low viscosity, pale yellow, molecular liquid where molecules are predominantly S_8 rings. With an increase in the temperature (at ambient pressure), the liquid undergoes a sudden increase of its viscosity near the so-called λ-transition, at T_λ= 432 K, a fact that is manifested in certain anomalies of many physical and chemical properties around this temperature.[33−37] These changes are known to be caused by a polymerization process involving the opening of sulfur rings to form diradical S_8 chains and the polymerization of these S_8^* fragments to long polymeric chains. The fascinating polymerization transition has been the focus of recent Raman scattering studies in an effort to investigate the temperature dependent monomer−polymer equilibrium.[38]

Glassy sulfur can be prepared by rapid quenching liquid sulfur as long as the liquid is heated at temperatures above the λ-transition. This means that the role of polymeric chains, which are in equilibrium with S_8 rings, is important for glassifying elemental S. In particular, g-S rapidly quenched from 473 K exhibits a glass transition temperature of T_g = 243 K.[39] Even traces of impurities can affect the polymerization transition of liquid sulfur[40] and its color.[33] It is therefore of paramount importance to carefully consider sulfur purification. Elemental sulfur (99.9995% purity) was further purified by repeated distillations into evacuated silica tubes. The final product in crystalline form was put in an Al sample holder with kapton windows and had a cylindrical shape of 1.3 mm thick and with a 5 mm diameter. The choice of the sample thickness has been

dictated by the need to match the photoelectric absorption length of sulfur at the chosen incident energy, and to therefore maximize the measured intensity.

The glassy sulfur has been obtained by first heating the crystalline powder up to 473 K and then by fast quenching the resulting polymeric liquid sulfur in liquid nitrogen. The sample has then been rapidly fixed on the coldfinger of a cryostat kept at 80 K. The glass quality has been checked during all the experiments by measuring the static structure factor of the system. In situ Raman studies of the polymer content have shown that ~45% of the mass fraction of liquid S at 473 K is in polymeric form, the rest being S_8 molecules.[38] Considering that quenching is fast enough so as to preserve to a large extent the polymer content of the liquid, it turns out that the polymer content of our glassy product is no more than ~45%.

3. DATA ANALYSIS

Figure 1 reports the dynamic structure factor of glassy sulfur measured at T = 202 K for selected exchanged wave vectors Q. The Brillouin doublet is well-defined close to the elastic line. On increasing the momentum transfer in the scattering process, the doublet clearly shifts toward higher energies and becomes broader. From the analysis of the spectra, it is possible to get information on the high frequency longitudinal sound velocity via the peak position and on the high frequency sound attenuation via the peak width. The intensity of the spectra is reported on an absolute scale following the procedure described below.

In general, the measured spectra can be formally expressed as[29]

$$I(Q,\hbar\omega) = A(Q)\breve{S}(Q,\hbar\omega) \quad (1)$$

where $\breve{S}(Q,\hbar\omega)$ is the dynamic structure factor, $S(Q,\hbar\omega)$, convoluted with the (normalized) instrumental function and $A(Q)$ is a normalization factor mainly reflecting the Q dependence of the atomic form factor. The dynamic structure factor can in turn be expressed in terms of its classical counterpart, $S^{cl}(Q,\hbar\omega)$:

$$S(Q,\hbar\omega) = \hbar\omega\frac{n(\hbar\omega)+1}{k_B T}S^{cl}(Q,\hbar\omega) \quad (2)$$

where $n(\hbar\omega)$ is the Bose factor. $S^{cl}(Q,\hbar\omega)$ can be modeled as the sum of a delta function to describe the elastic line and a damped harmonic oscillator model (DHO) for the inelastic component:

$$\frac{S^{cl}(Q,\hbar\omega)}{S(Q)} = f_Q\delta(\hbar\omega) + (1-f_Q)\frac{1}{\pi\hbar}\frac{\Omega(Q)^2\Gamma(Q)}{[\omega^2-\Omega(Q)^2]^2+\omega^2\Gamma(Q)^2} \quad (3)$$

where $S(Q)$ is the static structure factor, $\hbar\Omega$ is the excitation energy, $\hbar\Gamma$ is the fwhm, and f_Q is the nonergodicity factor that corresponds to the elastic to the total integrated intensity ratio. The IXS measured intensity has been fitted using the model function described by eq 3 in eqs 1 and 2. A baseline has also been added to account for background noise. In Figure 1, the experimental data are reported in terms of $(Q,\hbar\omega)$ together with the best fitting line shape, the DHO contribution corresponding to the inelastic features, and the instrumental resolution.

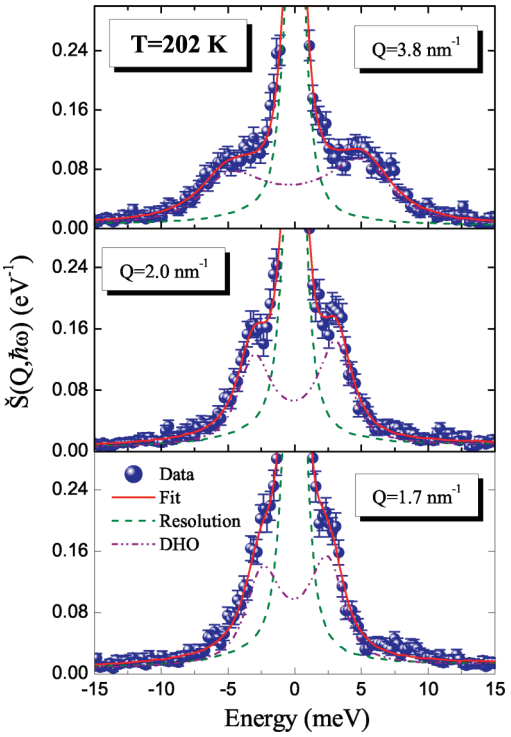

Figure 1. Selected IXS spectra of glassy sulfur at T = 202 K for different exchanged wave vectors Q together with the best fitting line shape (red line). The elastic (green line) and the inelastic (purple line) components of the DHO model are reported after convolution with the instrumental resolution. The intensity is reported on an absolute scale as explained in the text.

3.1. Spectra Normalization. The reliability of the measurements can be checked reporting the spectra on an absolute scale. In neutron scattering experiments, the measured spectra can be properly normalized using a reference scatterer. For IXS experiments, the situation is a bit more delicate, since geometrical effects can critically affect the relative intensity. Such a problem can be avoided using the frequency moments of the dynamic structure factor as a tool to normalize the measured intensity.[41] For such a purpose, the second moment is the most appropriate. In its classical formulation, it is given by the relation

$$M^{(2)}(Q) = \int_{-\infty}^{+\infty} d\omega\omega^2 S^{cl}(Q,\omega) = \frac{Q^2 k_B T}{M} \quad (4)$$

where k_B is the Boltzmann constant, T the temperature, ω the angular frequency, and M the molecular mass of the S_8 ring. The coefficient $A(Q)$ in eq 1 can be calculated exploiting eq 4 in the expression of the second moment of the experimental spectra, thus allowing us to bring the IXS spectra in absolute units (see Figure 1). This procedure allows also for the determination of the static structure factor $S(Q)$ by integrating the quantity $(1/A(Q))I(Q,\omega)$.

It is important here to stress that the whole procedure is an approximation, since the integration performed in the above equations is over the limited experimental energy range. The static structure factor has been calculated and is reported in the inset of Figure 2 together with the one directly measured during the experiment and corrected for the atomic form factor. The latter has been properly shifted in intensity in order to match the one estimated from the inelastic scattering spectra. The good

dx.doi.org/10.1021/jp2037075 |J. Phys. Chem. B 2011, 115, 14052–14063

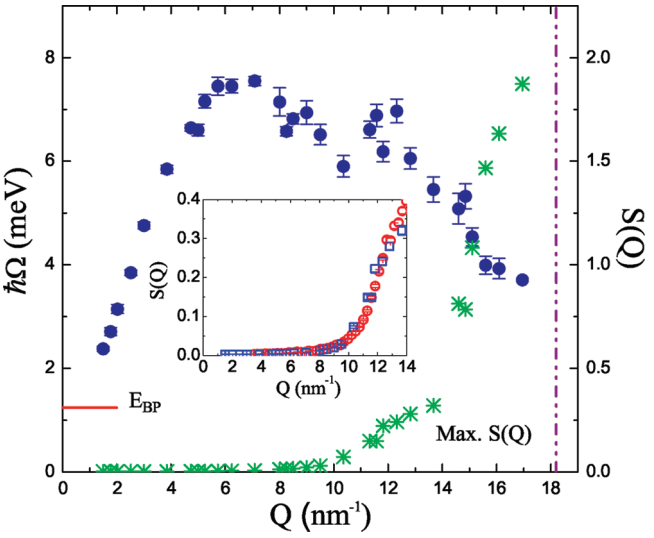

Figure 2. Dispersion relation of the longitudinal acoustic excitations of sulfur measured at T = 202 K. The data (blue dots) are reported as a function of the momentum transfer Q together with the static structure factor $S(Q)$ (green crosses) obtained from the integration of the spectra. The red line indicates the energy of the boson peak maximum, while the purple dashed line corresponds to the first sharp diffraction peak of $S(Q)$. Inset: Comparison between the measured $S(Q)$ corrected for the atomic form factor (red circles) and the one estimated using the zeroth moment rule of the $S(Q,\hbar\omega)$ (blue squares).

agreement at low Q is a confirmation of the whole normalization procedure.

A further check of this normalization procedure and, in particular, of the use of the DHO model (see eq 3) in the analysis of the spectra is given by the following equality

$$S(Q)(1 - f_Q) = \frac{k_B T}{M} \frac{Q^2}{\Omega(Q)^2} \quad (5)$$

between the inelastic intensity $S(Q)(1 - f_q)$ and the quantity $(k_B T/M)(Q^2/\Omega(Q)^2)$. In fact, this relation is just a consequence of the application of the second moment sum rule to the DHO model. The two sides of the equation have been calculated and the relation has been found to be well fulfilled in the whole investigated range, thus confirming the validity of our data analysis procedure.

4. RESULTS AND DISCUSSION

4.1. Acoustic Properties of Sulfur. Figure 2 reports the dispersion curve of sulfur for T = 202 K as a function of the exchanged momentum Q. The corresponding estimated static structure factor is reported as well (green dots). The dispersion curve displays a linear Q dependence for wave vector values up to ~6 nm^{-1}. At higher Q, the curve bends and monotonically decreases with increasing Q, up to the maximum of the static structure factor (dashed line in Figure 2). The red horizontal line in the figure represents the energy of the maximum of the boson peak (E_{BP} = 1.2 meV) obtained from the Raman measurements reported in Figure 3. In general, the Raman light scattering intensity can be written as[11]

$$I(\omega) = g(\omega)C(\omega)\frac{[n(\omega) + 1]}{\omega} \quad (6)$$

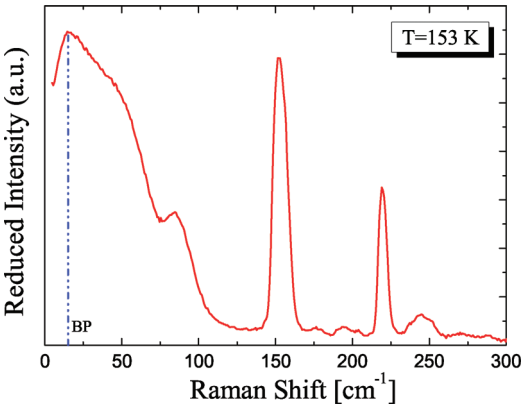

Figure 3. Reduced depolarized Raman intensity $I_R = C(\omega)g(\omega)/\omega^2$ of glassy sulfur at T = 153 K.

where $C(\omega)$ is the photon-vibration coupling coefficient, $n(\omega)$ is the Bose occupation factor, and $g(\omega)$ is the vibrational density of states. In Figure 3, the reduced Raman intensity $I_R = C(\omega)g(\omega)/\omega^2$ is reported. A maximum corresponding to the boson peak is well evident at about ~15 cm^{-1} (corresponding to 1.9 meV). This value does not coincide with the correct boson peak position, with I_R being related to the reduced vibrational density of states of a glass through the factor $C(\omega)$. The latter quantity is frequently considered to be proportional to the frequency ω. It is therefore obvious that the peak maximum of the BP in Raman scattering data will appear at higher frequencies than the BP measured in a neutron scattering experiment. In particular, the analysis of various experimental data shows that $E_{BP,Raman} \simeq 1.5E_{BP,neutrons}$ (see, for instance, the case of glassy selenium[42] and vitreous silica[43]). Considering this, we consequently estimate E_{BP} = 1.2 meV for glassy sulfur, the difference between $E_{BP,Raman}$ and E_{BP} being however irrelevant for all that follows here. This value is typical of fragile systems, such as polymeric glasses, and is out of the energy window accessible to IXS. In fact, as it is shown in Figure 2, the boson peak is located at a very low energy value with respect to the energy of the Brillouin peak at the lowest accessible Q. This means that an IXS experiment on glassy sulfur allows only the study of the high frequency dynamics well above the boson peak.

The upper panel of Figure 4 shows the apparent sound velocity, $v_L(Q) = \Omega(Q)/Q$, of sulfur at the three different investigated temperatures. The macroscopic limits measured with BLS[28] are reported as well as horizontal lines. There is no evidence of the negative dispersion found recently in several glasses.[29−31] The sound velocity of sulfur is almost constant up to $Q \sim 4$ nm^{-1} and then smoothly decreases on increasing the momentum transfer in the scattering process. A closer look shows that in reality a sort of anomaly in the case of sulfur is here observed. The high frequency sound velocity is in fact ~4% higher than the corresponding macroscopic limit (see inset in the upper panel of Figure 4). As explained in the next section, we ascribe this difference to the presence of an anharmonic contribution at low frequency which affects the values measured with BLS.

The lower panel of Figure 4 reports the width of the inelastic features as a function of the exchanged wave vector for the three temperatures. The data for the width do not also show the Q^4 Rayleigh-like behavior observed for other glasses in refs 29−31. The damping is temperature independent and follows the typical

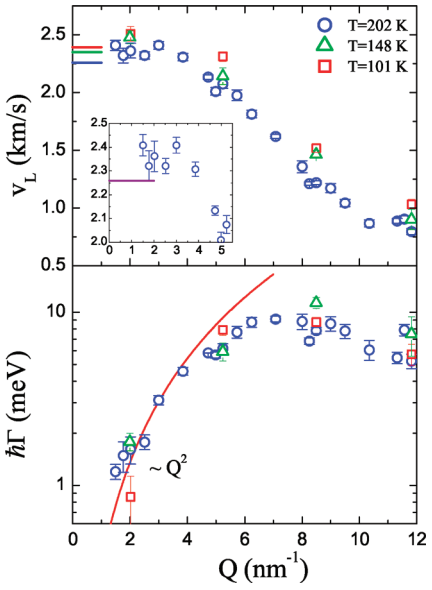

Figure 4. IXS results for the Q dependence of the sound velocity (upper panel) and broadening $\hbar\Gamma$ (lower panel) of the longitudinal acoustic excitations of glassy sulfur at the indicated temperatures. In the upper panel, the horizontal lines mark the macroscopic limits measured with BLS,[28] while the inset shows a zoom of the low Q behavior of the data taken at $T = 202$ K. In the lower panel, the red line is the quadratic best fit line shape for the low Q behavior of the data taken at $T = 202$ K.

$\sim Q^2$ behavior usually observed at energies higher than the boson peak.[44,45] On approaching the first sharp diffraction peak of $S(Q)$ (see Figure 2), the excitations become more and more ill-defined and $\hbar\Gamma$ deviates also from the observed quadratic dependence.

At first sight, the absence of elastic anomalies in the dynamics of sulfur seems to contradict the scenario reported in refs 29−31. However, this is not true. The existence of elastic anomalies at high frequency is strictly related to the boson peak, which, in the case of sulfur, is located at a value too low with respect to the minimum accessible energy value that can be probed with IXS (which corresponds to $Q \sim 1$ nm^{-1}, see Figure 2). In other words, the current experimental limitations of IXS do not allow the investigation of the character of the acoustic excitations of sulfur in the crucial energy range of the boson peak. Consequently, the data for sulfur remain in complete agreement with those obtained in other glasses at energies higher than that of the BP.

4.2. The Quasi-Harmonic Nature of the High Frequency Excitations. In order to understand the behavior of the high frequency sound velocity of sulfur, the data must be considered together with the corresponding attenuation data, $\hbar\Gamma$. These two quantities are in fact not independent: they are related to the real (M') and imaginary (M'') parts of the longitudinal elastic modulus $M(\omega) = M'(\omega) + iM''(\omega)$, being $M' = v_L^2\rho$ and $M'' = \Gamma v_L\rho/Q$, where ρ is the mass density.

The observed difference in glassy sulfur between the high frequency v_L measured with IXS and the low frequency one obtained from BLS measurements could be explained by the presence of an important anharmonic contribution at low frequency which would lead to a strong dispersion of the sound speed with frequency (or wavenumber). The strong temperature dependence of the low frequency sound attenuation reported in ref 28 is in fact a typical signature of the presence of an anharmonic contribution in the GHz frequency range explored by BLS.

In general, the role of anharmonicity can be quantitatively evaluated from the analysis of the low frequency longitudinal modulus. The temperature dependence of M' and M'' can be described taking into account two important contributions: (i) quasi-harmonic effects that induce a temperature dependence of the sound velocity following the dependence of density on temperature;[46,47] (ii) purely anharmonic effects that, as said above, play an important role on the acoustic absorption (and then on M'') in the GHz frequency range probed with BLS.[48] Following ref 49, it is then possible to set up a simple model to describe the BLS data. Indeed, the longitudinal modulus can be expressed as

$$M(\omega) = M_\infty - \frac{\Delta_M^2}{1 + i\omega\tau} \tag{7}$$

where $M_\infty = \rho v_\infty^2$ is the fully unrelaxed longitudinal modulus that one can measure at frequencies high enough for the anharmonic contributions to be completely negligible and v_∞ is the corresponding sound velocity; $\Delta_M^2 = M_\infty - M_{0\infty}$ represents the strength of the anharmonic process, where $M_{0\infty}$ is the fully relaxed longitudinal modulus that one would measure if there were no anharmonicity; and τ is an average relaxation time.[49] In this simple model, M' is then given by the quasi-harmonic term M_∞ corrected for the anharmonic contribution, while M'' is completely determined by the anharmonic term, being

$$M' = M_\infty - \frac{\Delta_M^2}{1 + \omega^2\tau^2} \quad \text{and} \quad M'' = \frac{\Delta_M^2\omega\tau}{1 + \omega^2\tau^2} \tag{8}$$

In the case of glassy sulfur, the lack of information on the temperature dependence of the density does not allow us to apply directly the model which, with $\Delta^2 = \Delta_M^2/\rho$, becomes

$$v_L^2 = v_\infty^2 - \frac{\Delta^2}{1 + \omega^2\tau^2} \quad \text{and} \quad \Gamma = \frac{\Delta^2}{v_\infty^2}\frac{\omega^2\tau}{1 + \omega^2\tau^2} \tag{9}$$

In these expressions, the quasiharmonic term is related to the fully unrelaxed sound velocity that we assume linearly dependent on temperature, i.e., $v_\infty = v_\infty^0(1 + aT)$. The anharmonic process is instead described by an average relaxation time $\tau = \tau_0 e^{(E_a/T)}$ and a strength given by $\Delta^2 = B(T - T_0)$, with $T_0 = 100$ K. This choice for the temperature dependence of Δ^2 is the simplest one compatible with the available information on the Brillouin line width of the longitudinal modes. In fact, due to the presence of cracks in the sample for temperatures lower than about 150 K, the line width of the longitudinal modes has been measured with BLS only for temperatures higher than 150 K (see Figure 5). The lack of data for Γ at lower temperatures does not allow us to formulate a more accurate model for the temperature dependence of the anharmonic contribution.

The best fitting curves obtained from this analysis are reported in Figure 5 together with the experimental data, while the fit parameters are reported in Table 1. The fit has been performed only in the temperature range where both Γ and v_L have been measured. The simple model described by eq 9 is clearly able to reasonably reproduce the experimental data, even if a more elaborate description would be necessary in order to account for the detailed shape of Γ. In particular, the model suggests that the sound velocity shows a relevant dispersion up to the THz frequency range probed by IXS, while the anharmonic contribution to the Brillouin width remains negligible in the high frequency range.

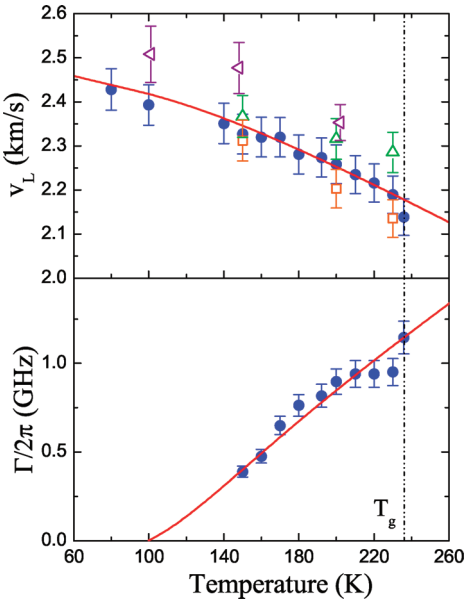

Figure 5. Temperature dependence of the sound velocity and fwhm of glassy sulfur measured with BLS[28] (blue circles). The red full lines are the best fitting curves using the model of eq 9. In the top panel, the fully relaxed $v_{0\infty}$ (orange empty squares) and unrelaxed v_∞ (empty green triangles) sound velocity values are reported for some representative temperatures, in order to emphasize the effect of anharmonicity. The high frequency IXS data of v_L (purple triangles) are plotted as well.

Table 1. Values of the Parameters of the Model (eq 9) Used to Describe the Temperature Behavior of $v_L(T)$ and $\Gamma(T)$ of Sulfur

v_∞^0 (km/s)	a (10^{-4} K^{-1})	B (m^2/s^{2}K)	τ_0 (ps)	E_n (K)
2.51	4.05	5.1	2.50	220

The strength of the anharmonic process yields information on the relaxed sound velocity $v_{0\infty}$, being $\Delta^2 = {v_\infty}^2 - {v_{0\infty}}^2$. The resulting values are also reported in Figure 5 at some selected temperatures together with the v_∞ values estimated from the fit. The low frequency dynamics of sulfur is clearly affected by a strong anharmonic contribution. On increasing the temperature, the strength of the anharmonic contribution increases and the measured sound velocities do not correspond any longer to the pure elastic limit measured at low Q with IXS (purple triangles in Figure 5). As a consequence, the macroscopic continuum limit of sulfur can be experimentally reached only at low temperatures or through the investigation of the dynamics at very high frequencies. The residual differences between the v_∞ value at $T = 150$ K and the corresponding IXS one are likely due to the limited accuracy in the high frequency estimation of v_L, which has been measured for only one Q value (see Figure 4). The same argument can be applied probably also to the IXS data at the lowest probed temperature, even though we do not have the estimated value for v_∞ there. This situation is similar to that observed in the case of a silicate glass.[25] In that system, in fact, the presence of anharmonic or relaxational processes at low frequency leads to a relevant dispersion of the sound velocity in the GHz range probed by BLS, so that the pure elastic limit can only be reached at high frequency.

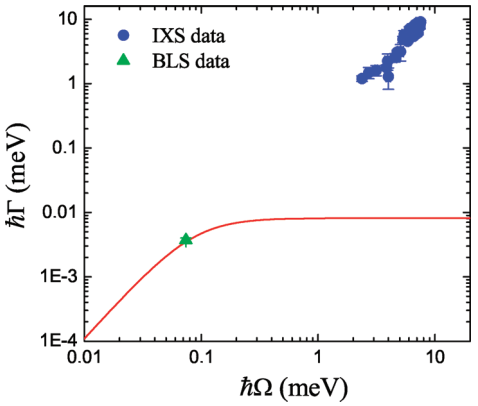

Figure 6. Brillouin width $\hbar\Gamma$ as a function of the excitation energy measured at $T = 202$ K with IXS (blue circles) and BLS (green triangle). The red line represents the anharmonic contribution to the damping, calculated from eq 9.

We can use the correct value v_∞ for the pure elastic limit to look with more detail at the low-Q behavior of the high frequency sound velocity measured at $T = 202$ K with IXS and reported in the top panel of Figure 4. We recall here that, in some recent IXS studies,[29−32] the longitudinal acoustic branch in different glasses has been shown to soften in the Q-range of a few nm^{-1} with respect to the macroscopic limit. Figure 4 shows that for sulfur the sound velocity seems to have already reached the macroscopic limit, being $v_\infty = 2350$ m/s. This would suggest the absence of any softening of the sound speed in this glass. However, in refs 29 and 32, it has been shown that the low-Q softening of the acoustic modes is responsible for the boson peak. As a consequence, depending on the intensity of the BP, we expect to find a more or less marked softening; in particular, the higher the BP intensity, the larger should be the softening of the sound velocity. It is recognized that the amplitude of the excess in the reduced VDOS is usually lower in fragile systems.[50] Even if we do not have information on the BP intensity of sulfur on an absolute scale, the presence of low elastic moduli, and of a high bulk to shear modulus ratio, B'/G', is typical of fragile systems having a BP less intense than that of systems, such as glycerol, silica, and sorbitol, where a clear negative dispersion has been found.[3,6,50] This ratio can be estimated by using the low frequency BLS data[28] and the shear modulus and the density of glassy sulfur reported in ref 39. We find $B'/G' = 7.7 \pm 0.3$, a value much higher than that typical of strong or intermediate glasses. For this reason, the negative dispersion in sulfur is expected to be weaker than that in the other systems, and could be hidden by the large scattering of the data at low Q (see top panel in Figure 4).

From the model (eq 9), we also find a value of $E_n \sim 220$ K and a characteristic time of $\tau \sim 7$ ps at $T = 200$ K. These values, together with the corresponding Δ^2 one, can be used to estimate the anharmonic contribution to the damping of the collective excitations at high frequencies. Figure 6 reports the Brillouin width $\hbar\Gamma$ measured at $T = 202$ K with IXS together with the anharmonic contribution calculated from eq 9 and the corresponding value measured with BLS. In the frequency range explored by IXS, the anharmonic contribution to the damping is expected to be almost 3 orders of magnitude smaller than the measured excitation broadening and can be completely neglected. This result confirms the non-dynamic nature of the sound attenuation in sulfur at high frequency.

dx.doi.org/10.1021/jp2037075 |J. Phys. Chem. B 2011, 115, 14052–14063

4.3. Compressibility and Nonergodicity Factor. The static structure factor obtained from the zeroth moment sum rule of $S(Q,\hbar\omega)$ can be used to estimate the isothermal compressibility, χ_T^0, of the corresponding supercooled liquid at T_g. In the case of equilibrium systems, such as liquids and gases, the macroscopic, $Q \rightarrow 0$, limit of the static structure factor gives information on the isothermal compressibility χ_T, being

$$S(Q \rightarrow 0) = \frac{\rho k_B T \chi_T}{M} \tag{10}$$

where ρ is the density.

In a glass, thus in a non-equilibrium system, this relation must be modified taking into account the relaxational processes that are frozen in at the glass transition temperature T_g.[51−53] By considering these nonpropagating density fluctuations that are kinetically arrested at T_g, the low Q limit of $S(Q)$ (eq 10) becomes

$$S(Q \rightarrow 0) = \frac{\rho k_B}{M}\{T_g[\chi_T^0(T_g) - M_\infty^{-1}(T_g)] + TM_\infty^{-1}(T)\} \tag{11}$$

where $M_\infty(T)$ is the real part of the high-frequency longitudinal modulus, related to the sound velocity of the acoustic modes through the relation $M_\infty(T) = \rho(T)v_\infty{}^2(T)$, and $\chi_T^0(T_g)$ is the isothermal compressibility in the liquid phase at the glass transition temperature.[54] The previous equation assumes, thus, that the fluctuations not frozen in below the glass transition arise from long-wavelength propagating vibrational modes due to high-frequency longitudinal excitations. In particular, the two relations eq 10 and eq 11 differ mainly in the case of fragile systems, such as polymeric systems, and less in strong materials. In fragile systems, in fact, the compressibility is characterized by a larger jump at the glass transition than in strong materials,[5] and only by properly considering this jump, it is possible to estimate the correct long wavelength limit of the density fluctuations.

By inverting eq 11, it is possible to obtain information on the isothermal compressibility, χ_T^0, of the corresponding supercooled liquid at T_g, being

$$\chi_T^0(T_g) = \frac{M}{\rho k_B T_g} S(Q \rightarrow 0) + M_\infty^{-1}(T_g) - \frac{T}{T_g} M_\infty^{-1}(T) \tag{12}$$

This quantity has been calculated as follows: the $S(Q \rightarrow 0)$ limit has been estimated using the IXS results on glassy sulfur at $T = 202$ K, the density has been assumed equal to the one measured below T_g ($\rho = 1.92$ g/cm^3),[55] and the values of M_∞^{-1} have been taken from the fully unrelaxed sound velocities v_∞ obtained from the analysis of the low frequency BLS data using the model (eq 9). We find $\chi_T^0(T_g) = 0.21 \pm 0.01$ GPa^{-1}.

This information can be used to estimate the long wavelength limit of the nonergodicity factor measured with IXS. For a system at thermodynamic equilibrium, the low-Q limit of the nonergodicity factor is given by the relation

$$f_Q(Q \rightarrow 0) = 1 - \frac{v_0{}^2}{v_\infty{}^2} \tag{13}$$

where v_0 and v_∞ are the relaxed and unrelaxed sound velocity, respectively. In the case of glasses, eq 13 should be modified by taking into account the jump of the isothermal compressibility at T_g. A correct macroscopic limit estimation should indeed consider the relaxational processes that are frozen in at the glass transition temperature as in the case of the static structure factor. By using the correct low Q limit for $S(Q)$ given by eq 11 and using eq 5, we obtain

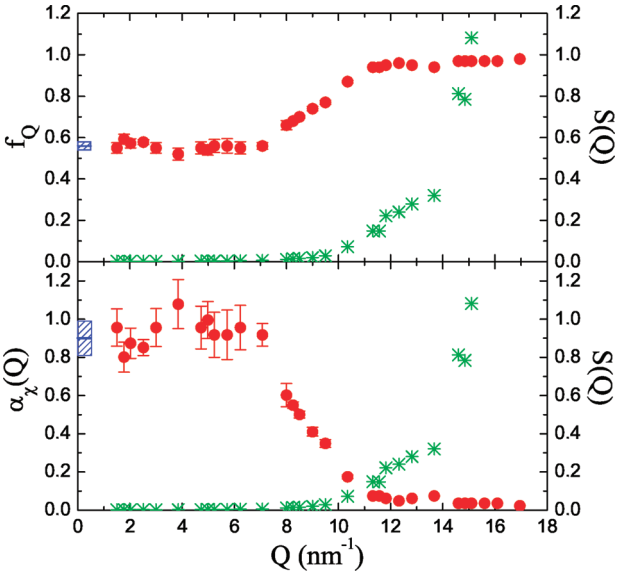

Figure 7. Top panel: Nonergodicity factor of sulfur measured at T = 202 K. The blue square represents the continuum limit given by relations 14 and 15. Bottom panel: Q dependence of the α_χ parameter obtained from eq 14. The blue rectangle is the continuum limit obtained through eq 15. The calculated $S(Q)$ is also reported in both panels (green stars).

$$f_Q(Q \rightarrow 0) = \frac{1}{1 + \alpha_\chi(T)\dfrac{T}{T_g}} \tag{14}$$

where the parameter $\alpha_\chi(T)$ is given by

$$\alpha_\chi(T) = \frac{M_\infty^{-1}(T)}{\chi_T^0(T_g) - M_\infty^{-1}(T_g)} \tag{15}$$

where $\chi_T^0(T_g)$ is the isothermal compressibility in the liquid phase at T_g and M_∞ the real part of the high frequency longitudinal modulus. Equation 14 is formally identical to the relation proposed by Scopigno and co-workers in ref 2. The main difference between these two relations resides in the definition of the parameter α_χ in the denominator. In the case of ref 2, this relation was deduced from an harmonic description of the atomic vibrations and the parameter α_χ (called α in ref 2) contains all the microscopic details of the system. In the present case, instead, the parameter α_χ is described only through macroscopic quantities and turns out to be nothing else than the extension for $T < T_g$ of the relation between the vibrational and relaxational compressibility proposed by Buchenau and Wischnewski.[5]

The nonergodicity factor of sulfur measured at T = 202 K is reported in the upper panel of Figure 7 together with the macroscopic limit given by eq 14. The f_Q of sulfur is basically flat in the low Q range, up to $Q \sim 7$ nm^{-1}, and corresponds to the macroscopic continuum value. This agreement confirms the validity of both the normalization procedure used for the IXS spectra and of the value obtained for χ_T^0 from eq 12. It in fact confirms that it is possible to get information on the isothermal compressibility of a supercooled liquid close to the glass transition

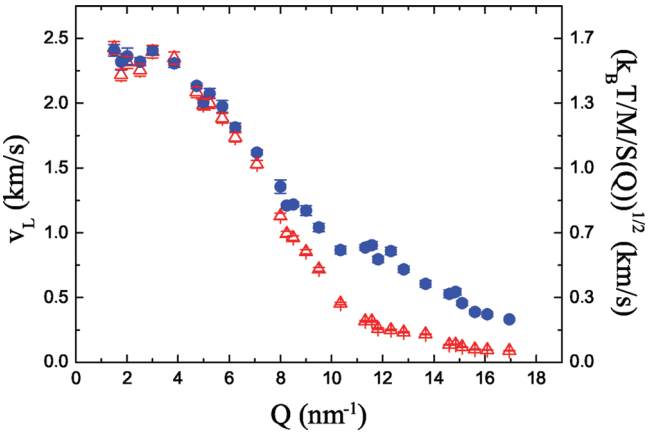

Figure 8. Wave vector dependence of the high frequency sound velocity v_L (blue circles, left axis) and $[k_BT/MS(Q)]^{1/2}$ (red triangles, right axis) of sulfur measured with IXS at T = 202 K.

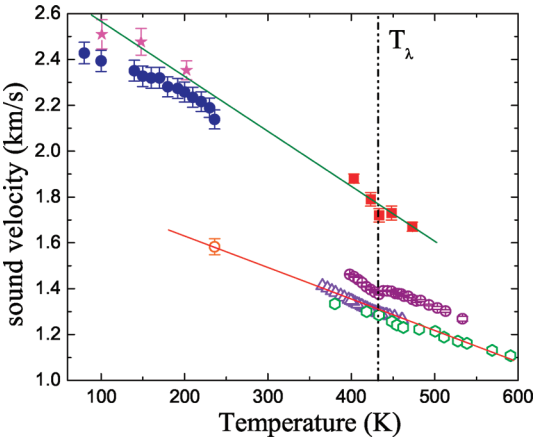

Figure 9. Temperature dependence of the sound velocity v_L of the longitudinal acoustic excitations. The values measured in the glassy state in the GHz (blue circles) and THz (magenta stars) frequency range are reported together with those measured in the liquid phase in the MHz (empty violet triangles and green hexagons),[56−58] in the BLS (empty purple circles),[59] and in the IXS (red squares)[60] frequency range. The orange empty circle has been calculated from the relation $v_0(T_g) = 1/[\rho(T_g)\chi_T^0(T_g)]^{1/2}$ using the values of $\chi_T^0(T_g)$ obtained from eq 12. The dashed black line indicates T_λ = 432 K. The red line shows that the value in the glass can be obtained by a simple linear extrapolation from those measured at very low frequency in the high temperature liquid phase above T_λ. The same kind of relation is valid also at high frequencies (full green line), where the high temperature data are compared with the pure elastic limit measured with IXS in the glass.

through the study of the vibrational dynamics in the corresponding glassy state.

The Q independence of the nonergodicity factor at low wave vectors implies that in the same Q range the shape of the high frequency sound velocity of sulfur is completely described by the Q dependence of the static structure factor. In fact, in this range, eq 5 yields $v_L \propto 1/(S(Q))^{1/2}$ (see Figure 8).

Equation 14 can be inverted to obtain the Q dependence of the $\alpha_\chi(Q)$ parameter, as shown in the lower panel of Figure 7, together with the corresponding long wavelength limit α_χ given by eq 15. The $\alpha_\chi(Q)$ parameter is equal to its macroscopic limit up to $Q \sim 7$ nm^{-1}, and then, it decreases on increasing Q. In the case of glassy sulfur, the low Q value corresponds thus to the correct α_χ value to be used to check the proposed correlation between the kinetic fragility of liquids and the vibrational dynamics in the glass.[2] The presence of a stronger Q dependence at low Q can be in fact the cause of some discrepancies in the proposed correlation between α_χ and the kinetic fragility.

4.4. Glassy Sulfur versus Liquid Sulfur. In a previous paper,[28] we have compared the sound velocity measured at low frequency with BLS in the glassy state with that corresponding to the liquid phase above and below the polymerization temperature T_λ (Figure 6 in ref 28). It is interesting here to add the new information obtained from the analysis of the high frequency dynamics of glassy sulfur.

Figure 9 displays the temperature dependence of the sound velocity measured in the GHz[28] and THz frequency range in the glassy state together with that measured in the MHz,[56−58] GHz,[59] and THz[60] frequency ranges in the liquid phase on crossing the λ transition. The differences observed in the liquid phase have been already discussed; therefore, we keep our attention on the comparison between the high frequency sound velocity in the polymeric liquid sulfur and the one measured in the corresponding glassy state. The two quantities are in fact strictly related and can be obtained one from the other through a simple linear extrapolation. However, due to the small but appreciable frequency dependence of the sound velocity at low frequency, it is more correct to compare the behavior of the high frequency polymeric liquid sulfur to that of the pure elastic limit measured at low Q and high frequency with IXS (magenta stars in Figure 9). As shown in the figure, even considering these data, the linear dependence of $v_\infty(T)$ is kept up to the high temperature polymeric liquid phase. This result confirms the strong relation between these two states of sulfur.

In the figure, we added also the point corresponding to the isothermal sound velocity $v_0(T_g) = 1/(\rho(T_g)\chi_T^0(T_g))^{1/2}$ estimated from the value of the isothermal compressibility of the liquid at T_g obtained from the analysis of the IXS data (see eq 12). Also in this case, this value can be linearly extrapolated from those measured at very low frequency in the high temperature liquid phase above T_λ.

4.5. Kinetic Fragility and Elastic Properties. In the last years, a lot of effort has been spent to connect the rapid increase of the structural α-relaxation time in the supercooled liquid phase, expressed by the different fragility metrics, to other properties of glass formers in both the liquid and glassy state. In particular, the discovery of a link between the slowing down of the diffusive motion in the supercooled liquid phase and the vibrational dynamics in the deep glassy state has intrigued many researchers.[2−8] This relation would imply, in principle, the possibility to get kinetic information on the structural α-relaxation time (or on the viscosity η) above T_g by studying the acoustic properties of the glass well below T_g. Despite the great amount of work done in this direction, the origin of these correlations is still not well understood and their validity is not unanimously accepted.[8,61]

To the best of our knowledge, no information on the kinetic fragility of polymeric sulfur is available in the literature. In the case of polymeric sulfur, the fragility cannot be directly estimated from the behavior of the viscosity (or the structural relaxation time) due to the presence of a secondary relaxation mechanism with comparable relaxation times.[62] This secondary relaxation

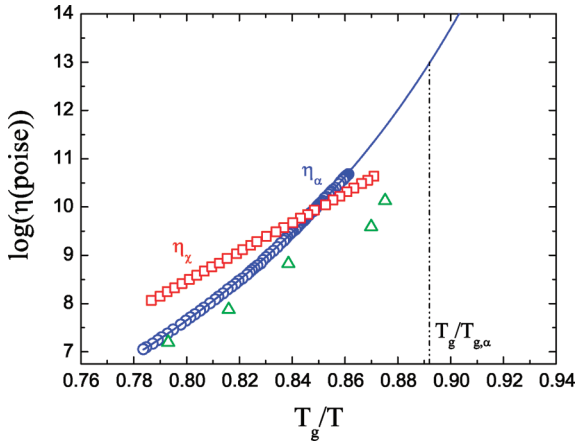

Figure 10. The total shear viscosity (green triangles) and the calculated viscosities due to the α (blue circles) and χ (red squares) relaxation mechanisms of polymeric sulfur as a function of the rescaled temperature T_g/T. The blue line is the best fit line shape using the WLF (eq 17) to determine the ideal glass transition temperature related to the α process as explained in the text. The data and the calculated viscosities are taken from ref 62.

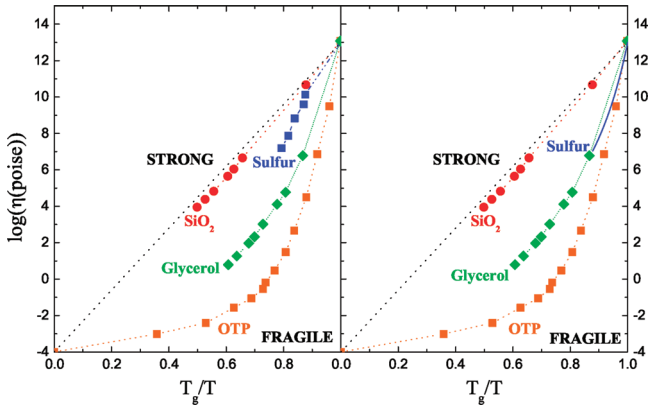

Figure 11. Left panel: Angell plot for several glass formers.[10] The data of sulfur correspond to the measured viscosity η (blue dots) and are reported as a function of the rescaled temperature T_g/T, using the dilatometrical glass transition temperature. Right panel: same data as for the left panel except for sulfur. In this case, only the α component of the viscosity is reported (blue line) as a function of the rescaled temperature T_g/T, using the ideal glass transition temperature $T_g = T_{g,\alpha}$ as explained in the text. The data for sulfur are taken from ref 62.

mechanism, called the χ process, has been studied in ref 62 and corresponds to a S−S bond interchange in small segments of the polymeric chains. As a consequence, the viscosity of the system contains a contribution additional to that related to molecular flow, and can be written as[62]

$$\frac{1}{\eta} = \frac{1}{\eta_\alpha} + \frac{1}{\eta_\chi} \tag{16}$$

where η_α and η_χ are the viscosities due to the α process and to the additional χ relaxation mechanism, respectively. Figure 10 reports the measured viscosity together with the values estimated in ref 62 for $(1/\eta_\alpha)$ and $(1/\eta_\chi)$ as a function of the rescaled temperature T_g/T.

It is important to note that the contribution to the viscosity of the secondary χ process becomes more and more important on approaching T_g, and becomes dominant close to T_g. We used this information to estimate the kinetic fragility m_A of polymeric sulfur. It is clear, indeed, that it cannot be directly calculated from the experimental data reported in Figure 10, which in fact would lead to a very low value of $m_A = [\mathrm{d}\log(\eta(T))/\mathrm{d}(T_g/T)]_{T=T_g} = 28 \pm 2$, very unusual for a polymeric system. A correct value of m_A should be related only to the α relaxation mechanism. In the case of polymeric systems, such as sulfur, the viscosity associated with the α-relaxation process is well described by the Williams−Landel−Ferry (WLF) equation[63]

$$\log(\eta_\alpha) = A + C_1\frac{T - T_g}{C_2 + T - T_g} \tag{17}$$

where A, C_1, and C_2 are fitting parameters. In general, $A = 13$ is related to the value of the viscosity at T_g, being $A = \log(\eta_\alpha(T_g))$. The best fit line shape of η_α using eq 17 and $T_g = 243$ K is reported in Figure 10. The obtained parameters are $A = 34 \pm 1$, $C_1 = -35 \pm 1$, and $C_2 = 19 \pm 1$. These values are in clear disagreement with the WLF equation model; in particular, A is almost 3 times larger than the expected value of 13. The corresponding kinetic fragility m_A can be written as

$$m_A = \left(\frac{\frac{-C_1C_2}{T_g}}{\left(\frac{C_2x}{T_g} + 1 - x\right)^2}\right)_{x=1} \tag{18}$$

with $x = T_g/T$. Using the obtained parameters, we find $m_A = 453$, which is an unreasonably high value. This apparent incongruity can be explained by the presence of the strong secondary relaxation mechanism close to T_g, where T_g has been obtained dilatometrically and does not correspond to the condition $\eta_\alpha(T_g) = 10^{13}$ poise. The fragility should instead be estimated with respect to the ideal glass transition temperature $T_{g,\alpha}$ related to the structural relaxation process by the condition $\log(\eta_\alpha(T_{g,\alpha})) = 13$ (dashed−dotted−dotted line in Figure 10). Using $T_{g,\alpha} = 276$ K (and thus $x = 0.892$), eq 18 gives $m_A = 86 \pm 7$. This estimation, typical of more fragile systems, can be considered as the reference value for the fragility of polymeric sulfur. Using the correct limit $\log(\eta_\alpha(T_{g,\alpha})) = 13$ and the estimated value for $T_{g,\alpha}$, the parameters of the WLF (eq 17) become $C_1 = -13.5 \pm 0.5$ and $C_2 = 48.1 \pm 0.2$. These values are very typical of other glass-forming systems and represent thus a confirmation of the validity of the whole procedure.[63]

The above observations are summarized in Figure 11, where sulfur is added to the well-known Angell plot.[10] In particular, the left panel shows the measured total viscosity η of sulfur as a function of the rescaled temperature T_g/T, using the dilatometric T_g, while in the right panel only the η_α contribution is reported by rescaling the temperature with $T_{g,\alpha}$. On including the secondary χ relaxation process, the η data are clearly shifted toward too high temperatures, leading thus to an "illusory" strong character of sulfur (left panel).

The obtained estimation of the kinetic fragility of liquid sulfur can be used to check the validity of the linear correlation $m_A = 135\alpha_\chi$ proposed in refs 2 and 64 between the kinetic fragility and the α_χ parameter obtained from the long wavelength limit of the

dx.doi.org/10.1021/jp2037075 |J. Phys. Chem. B 2011, 115, 14052–14063

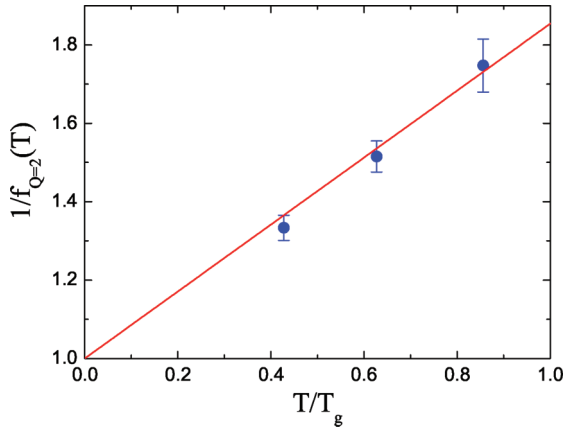

Figure 12. Inverse of the nonergodicity factor of sulfur for $Q = 2$ nm^{-1} measured at T = 101, 148, and 202 K as a function of the rescaled temperature T/T_g. The red line represents the best fit using the relation $1/f_Q = 1 + \alpha(T/T_g)$.

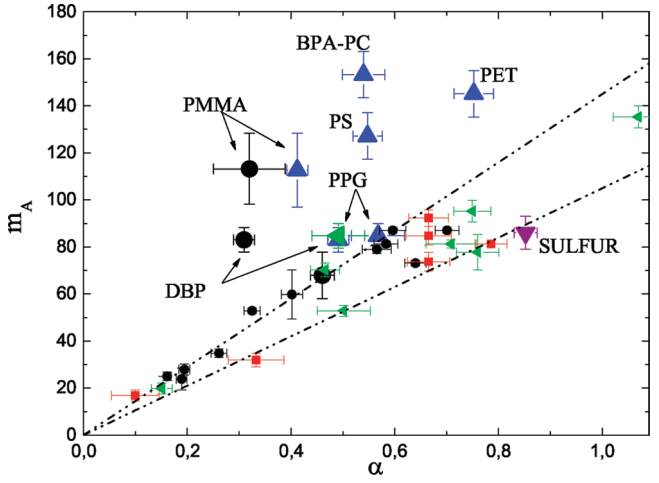

Figure 13. Correlation between the temperature dependence of the relaxation time (quantified by the kinetic fragility, m_A) and the nonergodicity factor (represented by the α_χ parameter of eq 14) for several glasses. Here, the parameter α_χ has been evaluated assuming that only the structural relaxation process contributes to the nonergodicity factor of the considered glasses. All the data are taken from ref 64 with the exception of sulfur, for which the α_χ parameter has been calculated from eq 15 (purple triangle). The data without a label are the same as in Figure 1 of ref 2.

temperature dependence of the inverse of the nonergodicity factor as a function of the rescaled temperature T/T_g.[2,5] The corresponding data for sulfur for $Q = 2$ nm^{-1} are reported in Figure 12 together with the best fit line shape which formally corresponds to eq 14. From the slope of the curve, we obtain a kinetic fragility of $m_{IXS} = 115 \pm 3$. This value is consistent within the experimental error bars with the one that can be estimated using directly the low-Q, macroscopic value of α_χ obtained from the data collected at T = 202 K (bottom panel of Figure 7).

In Figure 13, we add the information obtained for sulfur on the original correlation plot proposed between the kinetic fragility m_A and the α_χ parameter.[2,64] The value obtained for sulfur is consistent with the overall trend, which is in fact quite a bit scattered. As previously reported, it has been proposed that the originally proposed correlation[2] fails in many fragile systems due to the presence of relevant secondary relaxation processes, which affect the evaluation of the nonergodicity factor in the deep glassy state.[64] The presence of a secondary relaxation contribution adds in fact an extra part to the area of the elastic line in the $S(Q,\hbar\omega)$, leading to an incorrect evaluation of f_Q, and then of the parameter α_χ. Applying this correction to the directly derived values for the α_χ parameter, a good correlation between m_A and the corrected α_χ parameter seems to be recovered.[64] As shown by the viscosity measurements discussed here, sulfur is as well affected by a secondary relaxation, the χ one, which is particularly relevant close to T_g, so that the reasonably good correlation between α_χ and m_A shown in Figure 13 could sound a bit odd. However, to the best of our knowledge, no information on the strength of the χ relaxation in sulfur is available, so that the correction scheme proposed in ref 64 cannot be tested at the moment for the case of sulfur.

5. CONCLUSIONS

The vibrational properties in a partially polymeric glass of sulfur have been scrutinized in a wide frequency range in order to shed some light on different disputed topics concerning glass dynamics. Two main topics have been discussed: on one side, the elastic properties have been considered in relation to the excess in the VDOS known as the boson peak; on the other side, the proposed correlation between elasticity of the glass and fragility of the corresponding supercooled liquid has been investigated.

The knowledge of the dynamics on different length scales is found to be mandatory in order to fully understand the character of the acoustic excitations in the glass. In particular, the high frequency dynamics in sulfur does not show any signature of the elastic anomalies recently found in several glasses and which seem to be related to the boson peak.[29−32] The dispersion curve for sulfur follows the typical sine-like behavior as observed in several other systems,[44] while the acoustic attenuation exhibits an almost quadratic dependence on the excitation energy and is definitely non-dynamic in origin. Notwithstanding, this result is not in disagreement with the previous ones. In the case of glassy sulfur, the current experimental limitations of IXS and the low BP energy position do not allow for the investigation of the acoustic excitations in the crucial energy range of the BP. In sulfur, then the acoustic anomalies observed in other glasses are likely shifted toward lower energies in a range that cannot be explored at the current time. The behavior of the acoustic attenuation is in fact in agreement with that observed in refs 29−31 for energies higher than that of the BP. These considerations reconcile the present data with the scenario of universal elastic anomalies related to the BP, and can moreover explain why no signature of elastic anomalies has been previously found in other systems such as glassy ethanol[65] and Se.[66]

Some peculiarities are found in the IXS, high frequency sound velocity values with respect to the macroscopic limit explored with BLS that can be explained in terms of an anharmonic contribution which affects the acoustic properties in the GHz frequency range. This anharmonic contribution has been parametrized here to some extent.

By considering the correct long wavelength limit of the density fluctuations in the glassy state, we show that it is possible to estimate some macroscopic properties of the corresponding viscous melt at the glass transition, such as the isothermal compressibility and therefore the completely relaxed sound velocity. This information has been used to find the continuum

limit of the nonergodicity factor in the glassy state, that has been expressed by a natural extension of a relation originally proposed by Buchenau and Wischnewski.[5] The validity of the whole procedure is then confirmed by the very good agreement at low wave vectors between the nonergodicity factor obtained from the IXS spectra and its macroscopic value estimated by taking into account the presence of anharmonicity at low frequency. A further confirmation of our results is also obtained from the simple linear relation between the calculated relaxed sound velocity of polymeric liquid sulfur at T_g and the values measured at low frequency in the high temperature liquid above the λ transition.

Finally, the relation between the nonergodicity parameter and the kinetic fragility[2] has been studied for the case of sulfur. A correct investigation of this relation requires the knowledge of the long wavelength limit of the nonergodicity factor. The values of kinetic fragility and nonergodicity factor obtained for sulfur fall well within the general, though scattered, trend for the proposed correlation. The presence of anharmonic contributions at high frequency or a possible Q dependence of the nonergodicity factor at low wave vectors could be the cause of some discrepancies found in the literature on the proposed relation. Consequently, it is important to perform an accurate investigation of the elastic properties of glasses over a large frequency range before drawing definite conclusions. A recent paper reports that a quantitative correlation between fragility and nonergodicity parameter is recovered once the latter one is properly corrected for the contribution of secondary relaxations in the glass.[64] The lack of information on the strength of the secondary relaxation processes active in glassy sulfur does not allow us at the present stage to test this proposal.

AUTHOR INFORMATION

Corresponding Author
*E-mail: giulio.monaco@esrf.fr.

ACKNOWLEDGMENT

R. Verbeni and C. Henriquet are gratefully acknowledged for technical support.

REFERENCES

(1) Ruocco, G., Ngai, K. L., Eds. 6th International Discussion Meeting on Relaxations in Complex Systems. *J. Non-Cryst. Solids* **2011**, *357*, 241−782.
(2) Scopigno, T.; Ruocco, G.; Sette, F.; Monaco, G. *Science* **2003**, *302*, 849.
(3) Novikov, V. N.; Sokolov, A. P. *Nature* **2004**, *431*, 961.
(4) Dyre, J. C. *Nat. Mater.* **2004**, *3*, 749.
(5) Buchenau, U.; Wischnewski, A. *Phys. Rev. B* **2004**, *70*, 092201.
(6) Novikov, V. N.; Ding, Y.; Sokolov, A. P. *Phys. Rev. E* **2005**, *71*, 061501.
(7) Niss, K.; Alba-Simionesco, C. *Phys. Rev. B* **2006**, *74*, 024205.
(8) Niss, K.; Dalle-Ferrier, C.; Giordano, V. M.; Monaco, G.; Frick, B.; Alba-Simionesco, C. *J. Chem. Phys.* **2008**, *129*, 194513.
(9) Oldekop, W. *Glastech. Ber.* **1957**, *30*, 8.
(10) Angell, C. A. *Science* **1995**, *267*, 1924.
(11) Phillips, W. A., Ed. *Amorphous Solids: Low-Temperature Properties*; Springer: Berlin, 1981.
(12) Buchenau, U.; Nücker, N.; Dianoux, A. J. *Phys. Rev. Lett.* **1984**, *53*, 2316.
(13) Grigera, T. S.; Martýn-Mayor, V.; Parisi, G.; Verrocchio, P. *Nature* **2003**, *422*, 289.
(14) Pilla, O.; Caponi, S.; Fontana, A.; Goncalves, J. R.; Montagna, M.; Rossi, F.; Viliani, G.; Angelani, L.; Ruocco, G.; Monaco, G.; Sette, F. *J. Phys.: Condens. Matter* **2004**, *16*, 8519.
(15) Leonforte, F.; Boissière, R.; Tanguy, A.; Wittmer, J. P.; Barrat, J.-L. *Phys. Rev. B* **2005**, *72*, 224206.
(16) Schirmacher, W.; Ruocco, G.; Scopigno, T. *Phys. Rev. Lett.* **2007**, *98*, 025501.
(17) Duval, E.; Mermet, A.; Saviot, L. *Phys. Rev. B* **2007**, *75*, 024201.
(18) Shintani, H.; Tanaka, H. *Nat. Mater.* **2008**, *7*, 870.
(19) Rufflé, B.; Foret, M.; Courtens, E.; Vacher, R.; Monaco, G. *Phys. Rev. Lett.* **2003**, *90*, 095502.
(20) Rufflé, B.; Guimbretière, G.; Courtens, E.; Vacher, R.; Monaco, G. *Phys. Rev. Lett.* **2006**, *96*, 045502.
(21) Monaco, A.; Chumakov, A. I.; Monaco, G.; Crichton, W. A.; Meyer, A.; Comez, L.; Fioretto, D.; Korecki, J.; Ruffer, R. *Phys. Rev. Lett.* **2006**, *97*, 135501.
(22) Kalampounias, A. G.; Papatheodorou, G. N.; Yannopoulos, S. N. *J. Non-Cryst. Solids* **2006**, *352*, 4619.
(23) Andrikopoulos, K. S.; Christofilos, D.; Kourouklis, G. A.; Yannopoulos, S. N. *J. Non-Cryst. Solids* **2006**, *352*, 4594.
(24) Niss, K.; Begen, B.; Frick, B.; Ollivier, J.; Beraud, A.; Sokolov, A.; Novikov, V. N.; Alba-Simionesco, C. *Phys. Rev. Lett.* **2007**, *99*, 055502.
(25) Baldi, G.; Fontana, A.; Monaco, G.; Orsingher, L.; Rols, S.; Rossi, F.; Ruta, B. *Phys. Rev. Lett.* **2009**, *102*, 195502.
(26) Rufflé, B.; Ayrinhac, S.; Courtens, E.; Vacher, R.; Foret, M.; Wischnewski, A.; Buchenau, U. *Phys. Rev. Lett.* **2010**, *104*, 067402.
(27) Chumakov, A. I.; et al. *Phys. Rev. Lett.* **2011**, *106*, 225501.
(28) Ruta, B.; Monaco, G.; Scarponi, F.; Fioretto, D.; Andrikopoulos, K. *J. Non-Cryst. Solids* **2010**, *357*, 563.
(29) Monaco, G.; Giordano, V. M. *Proc. Natl. Acad. Sci. U.S.A.* **2009**, *106*, 3659.
(30) Ruta, B.; Baldi, G.; Giordano, V. M.; Orsingher, L.; Rols, S.; Scarponi, F.; Monaco, G. *J. Chem. Phys.* **2010**, *133*, 041101.
(31) Baldi, G.; Giordano, V. M.; Monaco, G.; Ruta, B. *Phys. Rev. Lett.* **2010**, *104*, 195501.
(32) Monaco, G.; Mossa, S. *Proc. Natl. Acad. Sci. U.S.A.* **2009**, *106*, 16907.
(33) Meyer, B. *Chem. Rev.* **1976**, *76*, 367.
(34) Bacon, R. F.; Fanelli, R. *J. Am. Chem. Soc.* **1943**, *65*, 639.
(35) Zengh, K. M.; Greer, S. C. *J. Chem. Phys.* **1992**, *96*, 2175.
(36) Greer, S. C. *J. Chem. Phys.* **1986**, *84*, 6984.
(37) West, E. D. *J. Am. Chem. Soc.* **1959**, *81*, 29.
(38) Kalampounias, A. G.; Andrikopoulos, K. S.; Yannopoulos, S. N. *J. Chem. Phys.* **2003**, *118*, 8460.
(39) Tobolsky, A. V.; MacKnight, W. M.; Beevers, R. B.; Gupta, V. D. *Polymer* **1963**, *4*, 423.
(40) Bacon, R. F.; Fanelli, R. *Ind. Eng. Chem.* **1942**, *34*, 1043.
(41) Boon, J. P.; Yip, S. *Molecular Hydrodynamics*; Dover Publications, Inc.: New York, 1991.
(42) Yannopoulos, S. N.; Andrikopoulos, K. S. *J. Chem. Phys.* **2004**, *121*, 4747.
(43) Fontana, A.; Dell'Anna, R.; Montagna, M.; Rossi, F.; Viliani, G.; Ruocco, G.; Sampoli, M.; Buchenau, U.; Wischnewski, A. *Europhys. Lett.* **1999**, *47*, 56.
(44) Sette, F.; Krisch, M. H.; Masciovecchio, C.; Ruocco, G.; Monaco, G. *Science* **1998**, *280*, 1550.
(45) Ruocco, G.; Sette, F.; Leonardo, R. D.; Fioretto, D.; Krisch, M.; Lorenzen, M.; Masciovecchio, C.; Monaco, G.; Pignon, F.; Scopigno, T. *Phys. Rev. Lett.* **1999**, *83*, 5583.
(46) Birch, F. J. *Geophys. Res.* **1960**, *65*, 1083.
(47) Birch, F. J. *Geophys. Res.* **1961**, *66*, 2199.
(48) Vacher, R.; Courtens, E.; Foret, M. *Phys. Rev. B* **2005**, *72*, 214205.
(49) Jäckle, J.; Pichï, L *J. Non-Cryst. Solids* **1976**, *20*, 365.
(50) Sokolov, A. P.; Rössler, E.; Kisliuk, A.; Quitmann, D. *Phys. Rev. Lett.* **1993**, *71*, 2062.

(51) Laberge, N. L.; Vasilescu, V. V.; Montrose, C. J.; Macedo, P. B. *J. Am. Ceram. Soc.* **1973**, *56*, 506.
(52) Wright, A. C.; Hulme, R. A.; Sinclair, R. N. *Phys. Chem. Glasses* **2005**, *49*, 59.
(53) Levelut, C.; Parc, R. L.; Faivre, A.; Brüning, R.; Champagnon, B.; Martinez, V.; Simon, J.; Bleyd, F.; Hazemanne, J. *J. Appl. Crystallogr.* **2007**, *40*, S512.
(54) Naoki, M.; Ujitaand, K.; Kashima, S. *J. Phys. Chem.* **1993**, *97*, 12356.
(55) MacKnight, W. J.; Tobolsky, A. V. *Elemental Sulfur*; Wiley: New York, 1965.
(56) Kozhenikov, V. F.; Payne, W. B.; Olson, J. K.; Macdonald, C. L.; Inglefield, C. E. *J. Chem. Phys.* **2004**, *121*, 7379.
(57) Kozhenikov, V. F.; Viner, J. M.; Taylor, P. C. *Phys. Rev. B* **2001**, *64*, 214109.
(58) Gitis, M. B.; Mikhailov, I. G. *Sov. Phys. Acoust.* **2001**, *13*, 251.
(59) Scarponi, F.; Fioretto, D.; Crapanzano, L.; Monaco, G. *Philos. Mag.* **2007**, *87*, 673.
(60) Monaco, G.; Crapanzano, L.; Bellisent, R.; Crichton, W.; Fioretto, D.; Mezouar, M.; Scarponi, F.; Verbeni, R. *Phys. Rev. Lett.* **2005**, *95*, 255502.
(61) Yannopoulos, S. N.; Johari, G. P. *Nature* **2006**, *442*, E7–E8.
(62) Eisenberg, A.; Teter, L. *J. Phys. Chem.* **1967**, *71*, 2332.
(63) Williams, M.; Landel, R.; Ferry, J. *J. Am. Chem. Soc.* **1955**, *77*, 3701.
(64) Scopigno, T.; Cangialosi, D.; Ruocco, G. *Phys. Rev. B* **2010**, *81*, 100202.
(65) Matic, A.; Masciovecchio, C.; Engberg, D.; Monaco, G.; Börjesson, L.; Santucci, S. C.; Verbeni, R. *Phys. Rev. Lett.* **2004**, *93*, 145502.
(66) Scopigno, T.; Leonardo, R. D.; Ruocco, G.; Baron, A. Q. R.; Tsutsui, S.; Bossard, F.; Yannopoulos, S. N. *Phys. Rev. Lett.* **2004**, *92*, 025503.